Molecular motors in new media

Lubbe, Anouk Sophia

Chapter 4: Molecular Motors in Aqueous Environments

In this chapter, the behaviour of molecular motors is investigated in aqueous environments. Two water soluble molecular motors were designed and their dynamic properties studied. One of these designs proved to be stable under physiological conditions, and UV-vis, NMR and fluorescence experiments were conducted. Additionally, the rotational properties of a molecular motor were examined in micelles, as a model for bilayers, vesicles and other apolar environments found in the cell.

This work will be submitted for publication. Manuscript in preparation.

4.1 Introduction

Rotary molecular motors based on overcrowded alkenes were first reported in 1999[1] and have since been the subject of detailed investigation. Especially in earlier years, a thorough understanding of the exact mechanism of rotation has been formed through extensive research.[2–4] Subsequently, the unique properties of molecular motors have found a myriad of applications. The inversion in helical chirality that accompanies each rotational step has been exploited to govern, among others, the outcome of asymmetric catalysis,[5] to induce unidirectional rotation of a microscopic glass rod[6] and to modulate preference for binding of chiral anions.[7] As molecular photoswitches, molecular motors are robust and highly efficient. The multiple switch states have been used to induce gel-solution transitions,[8] change the morphology of nanotubes[9] and influence protein secondary structure.[10] Surface functionalization[11–13] has opened the door to potential applications in information storage, in which the four-state switching cycle of molecular motors is of particular appeal, and may also be used for magnification of collective behaviour. Finally, the potential of unidirectional rotation has been perhaps most effectively demonstrated by the directional movement of a motorized nanocar across a copper surface.[14]

Among all these examples, there is one area of research that has remained largely unexplored. Despite the recent surge in interest in the application of photoswitches in biological systems and in pharmacology,[15] molecular motors are thus far left out of the arsenal that makes up the primary tools for photopharmacology and other biological applications. Directional motion is ubiquitous in biology and motor proteins, such as ATPase, kinesin and myosin, which have served as an inspiration in the development of artificial molecular motors. The application of synthetic rotary molecular motors in a biological setting may lead to a whole new level of control over biological function. Our group has reported one example of a molecular motor incorporated in a peptide, where photoswitching of the motor could induce structural changes.[10] However, the hybrid shows strong aggregation behaviour, which was attributed to the hydrophobic core of the motor. This observation revealed the primary issue regarding the application of molecular motors in aqueous medium, i.e. their insolubility in water.

All light-driven overcrowded alkene-based molecular motors, from first to third generation, share the same bulky aromatic core structure,[1,2,16] which renders them inherently hydrophobic. A second generation molecular motor, functionalized with alkyl and PEG chains, could be operated in water, but as this motor is an amphiphile, it formed large supramolecular aggregates.[9] Additionally, a surface-bound second generation motor was used to modulate surface wettability, but this application was strongly dependent on hydrophobic effects.[17] Harada and co-workers have reported a first generation molecular motor functionalized with short peptide sequences, which was studied using UV-vis spectroscopy in aqueous solution.[18] However, potential aggregation was not investigated. It is highly likely that these structure behave similar to the peptides reported by our group (*vide supra*) and experience aggregation.

The most straightforward approach to solving this problem and creating molecular motors fully soluble in water is to functionalize a molecular motor with polar, solubilizing groups. As an alternative approach, molecular motors could be operated in the membrane or other apolar environments in the cell. In a recent publication, a molecular motor was used as a highly efficient photoswitchable anion receptor.[19] Such a system shows real promise for application in membrane transport. However, photoswitching of molecular motors in the membrane has not yet been demonstrated.

In this chapter, the study of molecular motors under aqueous, physiologically relevant conditions is reported using two complimentary strategies. Firstly, a water-soluble molecular motor was designed and studied in water. Secondly, a molecular motor that is insoluble in water was solubilized using micelles, as a model system for the biological membrane. Together, these two systems provide a base for further research towards the application of molecular motors in various parts of the cell.

4.2 Water-soluble molecular motors

4.2.1 Design

The primary objective of this investigation was to design, synthesize and evaluate a molecular motor that is not only soluble in water, but can also perform unidirectional rotation. For the ease of synthesis, first generation molecular motors were used as the design. Because the hydrophobic aromatic core structure is of vital importance for the rotational properties and cannot be avoided without an extensive redesign of the rotary unit, the molecules were modified with charged residues to enable the solubility in water. Scheme 4.1 depicts two of the initial designs. Both structures **4.1** and **4.2** are easily accessible by standard synthetic procedures.

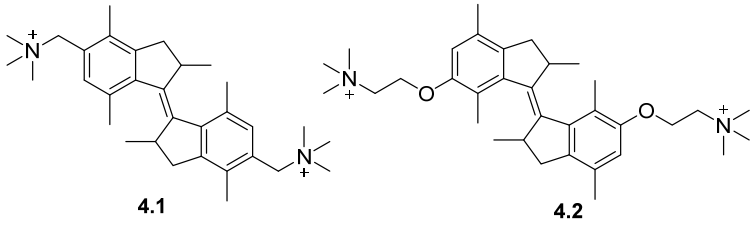

Scheme 4.1: Structures of proposed water-soluble motors.

4.2.2 Synthesis

Scheme 4.2 depicts the synthesis of water-soluble motor **4.1**. The synthesis was started from a mixture of *cis* and *trans* isomers of bromo-functionalized motor **2.7** (Chapter 2). The motor could easily be lithiated by addition of 3.5 equivalents of *n*-butyllithium, after which quenching with dimethylformamide led to formation of the dialdehyde product **4.3**. In this stage, the isomers could be easily separated using column chromatography. The aldehyde functionalities were converted to tertiary amines through reductive amination with dimethylamine and sodium trisacetoxyborohydride. Finally, water soluble motor **4.1** could be obtained by rapid quarternization using methyl iodide, after which the precipitated product could simply be filtered off.

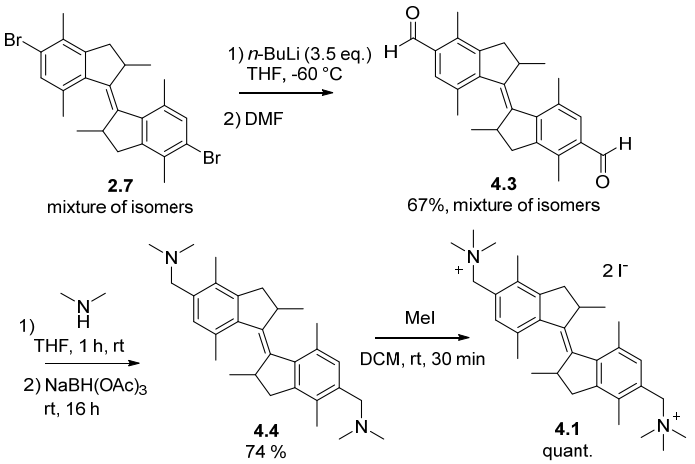

Scheme 4.2: Synthesis of water-soluble motor **4.1**. Only *trans* isomer depicted for clarity.

Scheme 4.3 depicts the synthesis of water-soluble motor **4.2**. The synthesis was started from phenolic motor **4.5**, which was reported previously.[20] Molecular motor **4.5** was synthesized in three steps on a large scale, and *cis* and *trans* isomers were separated using flash column chromatography. Dibromine-functionalized motor **4.6** was synthesized in near quantitative yield using standard Williamson etherification in the presence of an excess of dibromoethane. Subsequently, quarternization with trimethylamine generated the product **4.2**, which was easily precipitated out of organic solution.

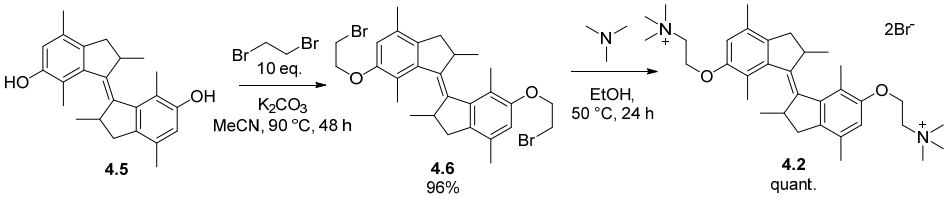

Scheme 4.3: Synthesis of first generation motor **4.2**. Only *trans* isomer depicted for clarity. *Cis*-**4.2** can be obtained by the analogous procedure.

4.2.3 Analysis of motor **4.1**

4.2.3.1 ^{1}H NMR analysis

The rotational behaviour of motor *trans*-**4.1** was investigated using ^{1}H NMR spectroscopy. Initially, a sample prepared in buffered D_2O (20 mM KPi buffer, prepared through repetitious lyophilisation and adding D_2O from pH = 7.2 buffer) was irradiated with 312 nm UV light for 30 min at 5 °C. The NMR spectrum revealed that the motor had completely degraded. The experiment was repeated, but this time the sample was analysed with 5 min intervals. Figure 4.1i shows the NMR spectrum of stable *trans*-**4.1**. After 15 min, several new peaks had appeared, which might indicate the formation of the unstable *cis* isomer (Figure 4.1ii). However, after 1 day at rt these peaks did not decrease, as would be expected if thermal helix inversion had occurred (Figure 4.1iii). Additionally, no new peaks corresponding the stable *cis* isomer appeared.

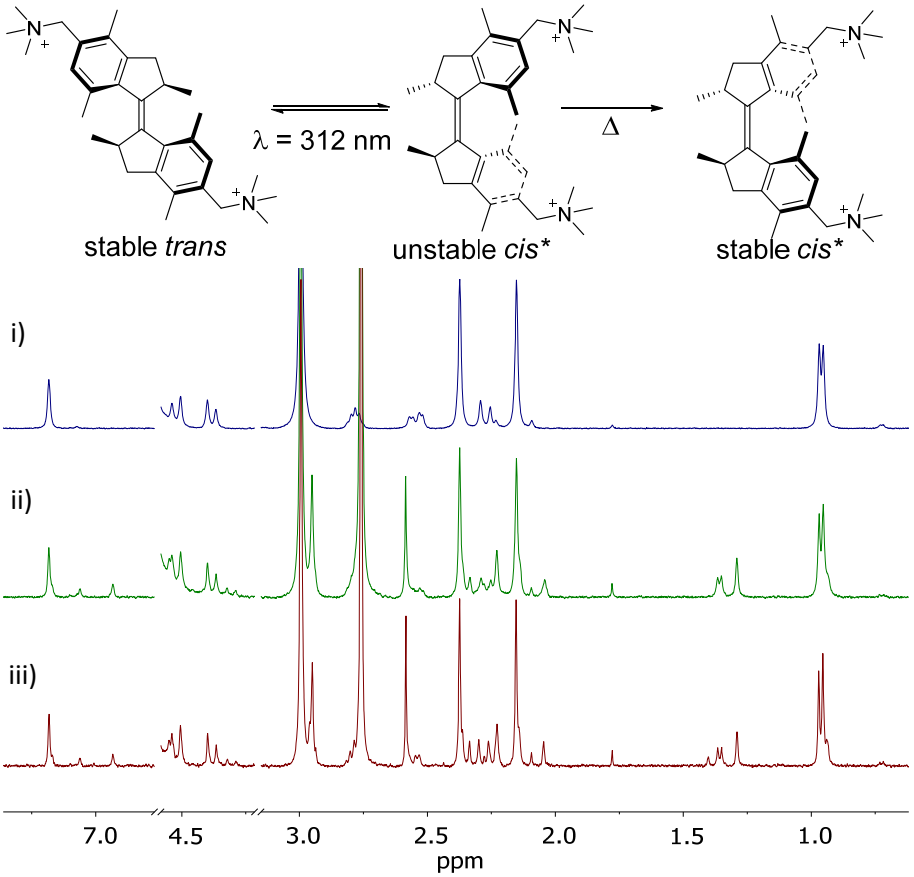

Figure 4.1: NMR experiments in buffered D_2O (20 mM KPi, pH = 7.2, 400 MHz, 20 °C). i) Stable *trans*-**4.1**, ii) Sample after 15 min of irradiation (312 nm, 5 °C), iii) Sample after heating to rt for 1 d, consisting of a mixture of stable *trans*-**4.1** and side product. * Indicates expected products. No stable *cis* identified in NMR spectrum.

4.2.3.2 UV-vis spectroscopy

Figure 4.2 depicts the UV-vis analysis of *trans*-**4.1**. The motor was dissolved in buffer (25 mM Tris, Bis-Tris, MES and sodium acetate, pH= 7.4) and a UV-vis spectrum was recorded (Figure 4.2 a, black line). Subsequent irradiation with 312 nm light led to appearance of an absorption band at a higher wavelength, consistent with the formation of the unstable *cis* isomer. However, the absence of an isosbestic point indicates the occurrence of side reactions. Subsequently, the sample was left at room temperature and conversion was monitored after one day, and again after three days (Figure 4.2b). Thermal helix inversion is typically accompanied by a disappearance of the higher energy absorption band, and an increase of absorption at lower wavelengths. However, in this sample the absorption was gradually decreasing at all wavelengths. Therefore, degradation of the motor is more likely. Nucleophilic attack of the benzylic position, with NMe_3 as a leaving group, is a likely cause of this degradation. The insoluble product of this reaction (presumably a diol) would precipitate out of the solution, which is in accordance with the decrease in absorbance observed in Figure 4.2b. Based on the combined results of the UV-vis and ^{1}H NMR analysis, it was decided that motor **4.1** was unsuitable to be operated in aqueous solutions.

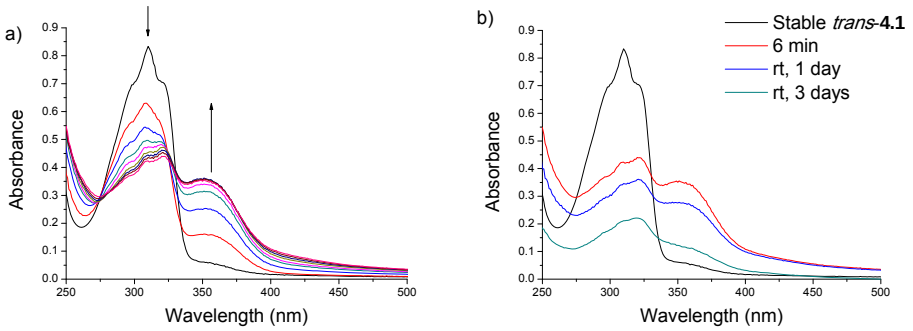

Figure 4.2: UV-vis analysis of rotational behaviour of motor **4.1** in buffer (Bis-Tris, MES, Tris and sodium acetate, 25mM each, pH = 7.4). (a) Irradiation from stable *trans*-**4.1** (black line), 312 nm, 6 min, 20 °C. (b) Stable *trans*-**4.1** (black line), sample after 6 min of irradiation (red line), and after leaving the sample at room temperature for 24 h (blue line) and 72 h (turquoise line).

4.2.4 Analysis of motor **4.2**

4.2.4.1 ^{1}H NMR analysis

The rotational behaviour of motor **4.2** was investigated using ^{1}H NMR spectroscopy. Only the 180° rotation from stable *trans* to stable *cis* was studied. The half-life of the unstable *trans* isomer is expected to be < 10 s at rt, and therefore this isomer is considered unsuitable to be studied in aqueous environment, since low temperatures (below the freezing point of water) would have to be used. Figure 4.3 depicts the ^{1}H NMR analysis of the isomerization of stable *trans*-**4.2** in buffered D_2O (20 mM KPi, pD = 7.2). For clarity, the aromatic hydrogen atoms and the methyl groups at the stereogenic cen-

tres are highlighted. After 45 min of irradiation, a ratio of ~ 4:1 unstable *cis*/stable *trans* was measured (Figure 4.3iii). Irradiation was halted, because several new peaks appeared, indicative of slow degradation. Subsequently, the sample was left at rt for 5 days (Figure 4.3iii). All unstable *cis* isomer converted to the stable *cis* isomer, and no additional degradation was observed.

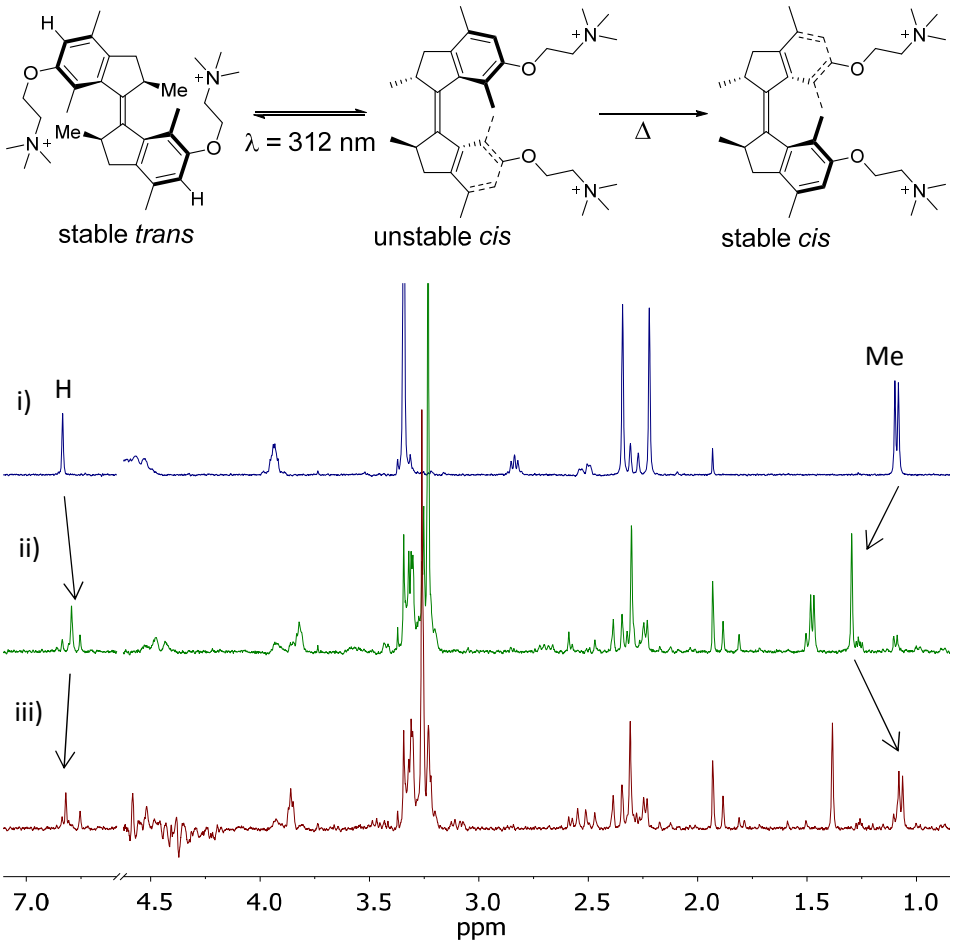

Figure 4.3: NMR experiments in buffered D_2O (20 mM KPi, pD = 7.2, 400 MHz, 20 °C). i) Stable *trans*-**4.2**, ii) Sample after 45 min of irradiation (312 nm, 5 °C), iii) Sample after heating to rt for 5 d, consisting of a mixture of stable *cis*-**4.2**, stable *trans*-**4.2**, and degradation product(s). Relevant peaks are indicated with arrows.

4.2.4.2 UV-vis spectroscopy

The rotational process was subsequently studied using UV-vis spectroscopy. A solution of stable *trans*-**4.2** in PBS buffer was irradiated under air using 312 nm UV light (Figure 4.4a). The appearance of a new band at higher wavelengths is indicative of the formation of the unstable *cis* isomer. A clear isosbestic point at 330 nm indicates the absence of unwanted side reactions. After 12 min of irradiation, a minor isosbestic point shift was observed (Figure 4.4a) and the irradiation was halted (Figure 4.4b, red line). The sample was subsequently left at room temperature overnight. The new band disappeared and the band below 325 increased in absorption (Figure 4.4b, blue line). These changes are indicative of the THI and generation of a lower energy isomer (stable *cis*).

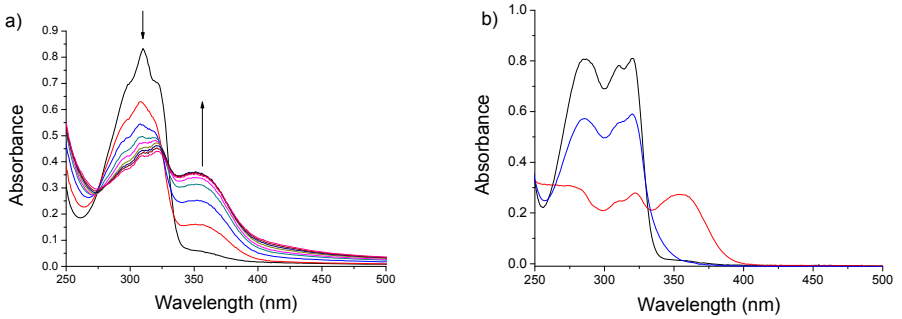

Figure 4.4: UV-vis analysis of rotational behaviour of motor **4.2** in PBS buffer (pH = 7.4). (a) Irradiation from stable *trans*-**4.2** (black line), 312 nm, 12 min, 20 °C. (b) Stable *trans*-**4.2** (black line), sample after 12 min of irradiation (red line), and after subsequent THI at room temperature overnight (blue line).

By measuring the speed of the THI at various temperatures, an Eyring plot was constructed and the activation parameters of the unstable *cis* to stable *cis* conversion were calculated. The half-life of the unstable *cis* was found to be 22.8 h at rt and 18.5 min at human body temperature.

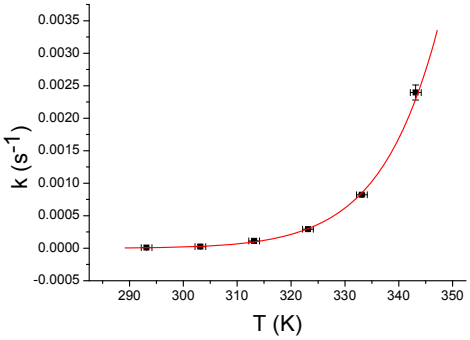

$\Delta^{\ddagger}H° = 101.0\pm0.0$ kJ/mol

$\Delta^{\ddagger}S° = -31.1\pm1.6$ kJ/mol

$\Delta^{\ddagger}G° = 91.1\pm0.8$ J/K/mol

Figure 4.5: Eyring plot for the thermal helix inversion from unstable *cis*-**4.2** to stable *cis*-**4.2**, and the calculated activation parameters (right).

4.2.4.3 Circular dichroism spectroscopy

To complement the UV-vis spectroscopic measurement, the 180° rotation from stable *trans*-**4.2** to stable *cis*-**4.2** was also followed in aqueous PBS buffer (pH = 7.4) using CD spectroscopy. The (*S*,*S*) enantiomer of stable *trans*-**4.2** was obtained through chiral resolution[20] and subsequently converted to stable *trans*-**4.2** using the same synthetic methodology as for the racemic motor (*vide supra*). Stable *trans*-*S*,*S*-**4.2** (Figure 4.6, black line) is homochiral with a specific optical rotation ($[\alpha]_D$ = 51.2° (c 0.5, methanol)). After irradiation with 312 nm light for 3 min, the photostationary state (PSS) was formed (Figure 4.6, red line). The higher wavelength band that is associated with formation of the unstable *cis* isomer induced a negative optical rotation, which is consistent with helicity inversion. After THI, the new band disappears and positive optical rotation is again observed (Figure 4.6, blue line).

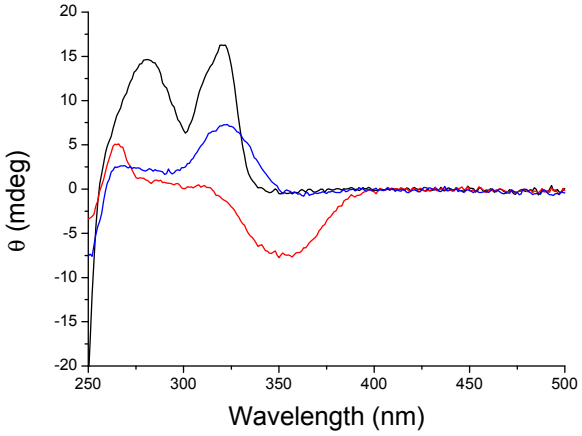

Figure 4.6: Circular dichroism spectra of isomers of motor **4.2** in PBS buffer (pH = 7.4). Stable *trans*-(*S*,*S*)-**4.2** (black line), PSS at 312 nm (red line), and after THI at rt (blue line).

4.2.4.4 Nile Red fluorescence assay

Molecular motor **4.2** appears to dissolve fully in aqueous media, and the absence of scattering effects at higher wavelengths in the UV-vis spectrum (Figure 4.4) suggests that no aggregates are present in solution. However, due to the large aromatic core, motor **4.2** may behave as an amphiphile or bolaamphiphile at higher concentrations. The potential aggregation behaviour of motor **4.2** was investigated using a fluorescence spectroscopy assay. Nile Red is a hydrophobic dye, which is poorly soluble in water and weakly fluoresces at around 660 nm.[21] In apolar environments, such as micelles or bilayers, the dye is soluble, which causes a strong increase in fluorescence and a blue-shift of the emission spectrum. In Figure 4.7, the λ_{max} of the emission spectrum of Nile Red in the presence of both isomers of motor **4.2** is depicted. Concentrations of motor were varied between 40 µM and 2.5 mM; the concentration of Nile red was ~1 µM for

each sample. As expected, both isomers appear to be fully soluble at concentrations below 0.1 mM, as demonstrated by the plateau around 660 nm. However, at higher concentrations, both isomers appear to aggregate, with a critical aggregation concentration of 1.0 mM for the *cis* isomer and 1.1 mM for the *trans* isomer. Notably, the sigmoidal curve is much steeper for the *cis* isomer than for the *trans* isomer. The reason for this difference is not clear, but the difference in aggregation behaviour may be used to create responsive aggregation at concentrations around the 1.0 mM.

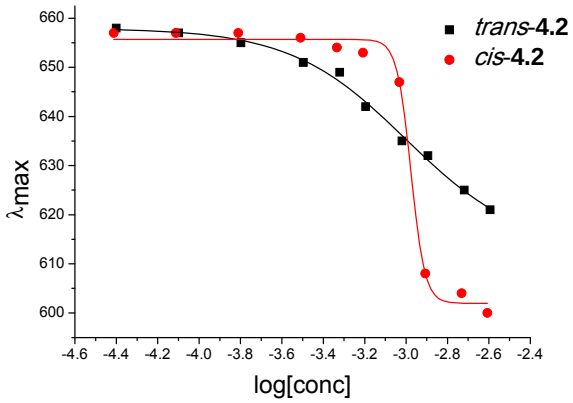

Figure 4.7: Emission of Nile Red in the presence of motor **4.2**, dissolved in buffer at pH = 10. Excitation wavelength is 550 nm.

4.2.4.5 Synthesis and analysis of a model compound for studying the possible decomposition pathway

Using a combination of techniques, it has been established that water-soluble overcrowded alkene **4.2** is soluble in aqueous solution, and functions as a molecular motor. However, the appearance of unidentified peaks in the NMR spectrum (Figure 4.3) and a small isosbestic point shift in the UV-vis spectra (Figure 4.4) indicate that some degradation is occurring. To identify the nature of the degradation, the NMR experiment was repeated in deuterated methanol. In this sample, the switching process was clean and no formation of side product was observed. It seems therefore that water is involved in the degradation. The most likely pathways for water-induced degradation are water addition to the central double bond and Hoffman elimination occurring on the quarternary ammonium bearing side chains. A model compound was designed to study the influence of UV irradiation in water on the solubilizing side chain. The synthesis was started from 1-(2-bromoethoxy)-naphthalene, which was previously reported by You and co-workers.[22] Quarternization, analogous to the manner previously reported by Singer and co-workers,[23] led to formation of model compound **4.7** in 60% yield (see Scheme 4.4). Model compound **4.7** was irradiated in water for 24 h with 312 nm UV light. The compound was stable under these conditions. Therefore, it seems that the solubilizing side chains are not responsible for the degradation.

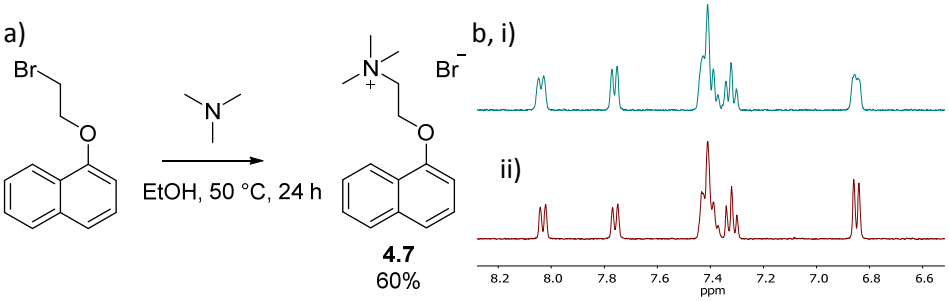

Scheme 4.4: (a) Synthesis of model compound **4.7**. (b) ^{1}H NMR analysis of model compound **4.7** (aromatic region shown)(i) **4.7** in D_2O, (ii) Sample after irradiation with 312 nm light, for 24 h.

4.2.4.6 UV-vis spectroscopy under varying atmospheres

A small isosbestic point shift was observed in the UV-vis spectrum of stable *trans*-**4.2** upon irradiation for several minutes (Figure 4.4a). Therefore, we were intrigued to see the effect of prolonged irradiation. A sample of stable *trans*-**4.2** in buffer (pH = 7.4) was irradiated with 312 nm light (Figure 4.8a). After initial appearance of the red-shifted band, the entire spectrum decreased in intensity. After 15 min, all absorption above 300 nm had almost entirely disappeared. Notably, all our experiments are performed under air, because we envision future applications under biologically relevant conditions. Oxygen might cause degradation of the motor. Therefore the experiment was repeated under an argon atmosphere. A buffer solution was degassed by performing three consecutive freeze-pump-thaw cycles and subsequently purged with argon for 30 min. The irradiation experiment was repeated under otherwise identical condition, but a similar degradation was observed (Figure 4.8b). Therefore, it seems unlikely that oxygen is involved in the degradation process. It is interesting to note that in both examples, a significant amount of unstable *cis*-**4.2** is generated first, and that the degradation sets in only after several minutes. The isosbestic point that can be observed during the first approx. 5 min of the irradiation process indicates that no unwanted side reaction occurs. Thus, it seems unlikely that a reaction intermediate of the photoisomerization is undergoing the degradation process. Moreover, if the irradiation is halted after the first indication of an isosbestic point shift, THI occurs (see Figure 4.4 and Figure 4.6). Therefore, the degradation seems to be the product of irradiation of the unstable *cis* isomer. Most likely, the degradation in water derives from some photogenerated reaction intermediate, such as a biradical state.

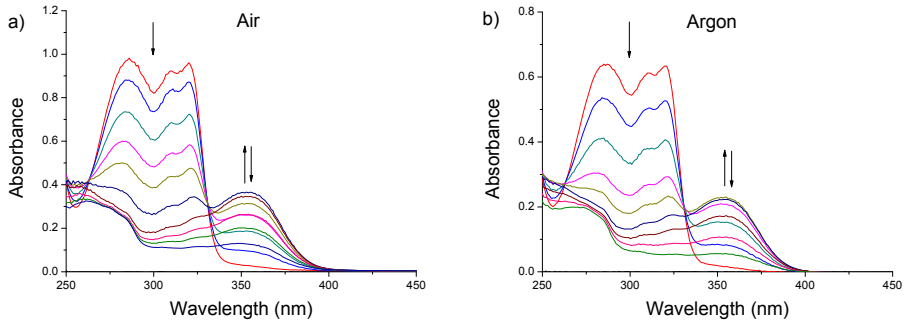

Figure 4.8: UV-vis spectra of stable *trans*-**4.2** in buffer (pH = 7.4), irradiated with 312 nm in different atmospheres. (a) Air. (b) Argon.

4.2.4.7 UV-vis spectroscopy over a pH range

Molecular motors are prone to degradation under strongly acidic conditions.[10] Therefore, we decided to investigate the influence of pH on the photoisomerization and THI of motor **4.2** (Figure 4.9). The irradiation experiment was performed in buffer solutions at pH = 2, 4, 6, 8, and 10, and additionally in unbuffered Milli-Q. The samples (stable *trans*-**4.2**, ~20 µM) were irradiated with 312 nm light at 20 °C for several minutes. All samples exhibit identical behaviour. Initially, a red-shifted absorption band appears, followed by a general decrease in absorption over the whole spectrum. The measurements indicate that de degradation is independent of pH.

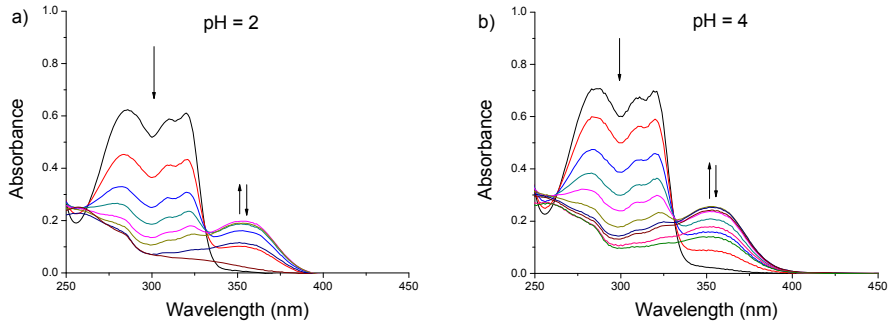

Figure 4.9: Stable motor *trans*-**4.2**, irradiated with 312 nm light in buffer (a-e) at varying pH or in unbuffered Milli-Q.

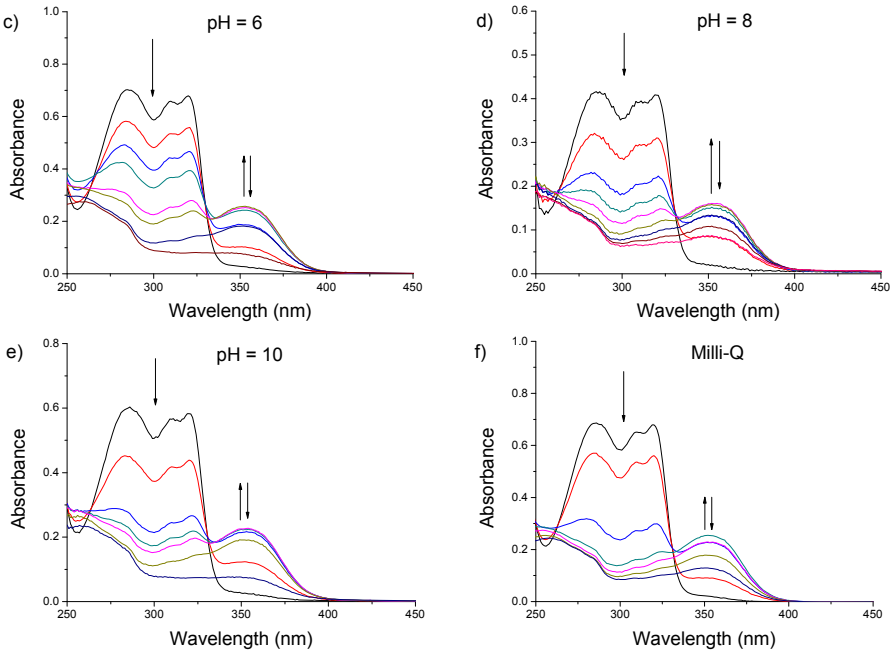

Figure 4.9 (continued): Stable motor *trans*-**4.2**, irradiated with 312 nm light in buffer (a-e) at varying pH or in unbuffered Milli-Q.

To assess the stability of non-irradiated stable *trans*-**4.2** in solution, a second set of samples covering the full pH range was prepared (Figure 4.10). The samples were monitored using UV-vis spectroscopy after one week, and no degradation was observed. Subsequent irradiation of the samples with 312 nm light caused isomerization followed by degradation as observed in all other samples. LCMS analysis of the samples showed the presence of two major species: 680 g/mol (motor **4.2**) and M+18. This result is consistent with the addition of water to the motor.

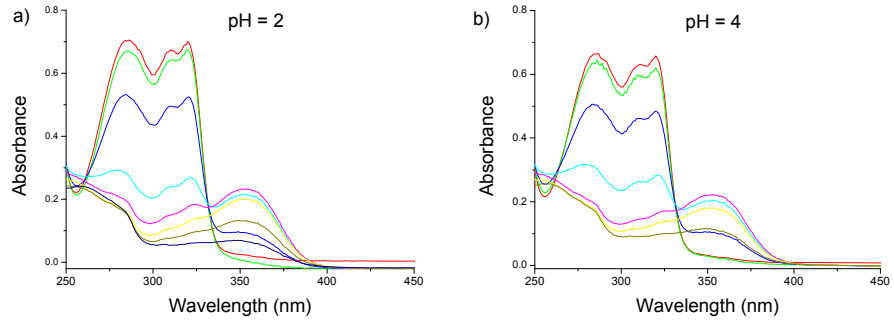

Figure 4.10: Motor **4.2** (a-e) at varying pH or in unbuffered Milli-Q (f). Stable *trans*-**4.2** (red lines), stable *trans*-**4.2** after 1 week (green lines) and subsequent irradiation (other lines). Despite careful control of analysis conditions, some baseline shifting is observed in several samples.

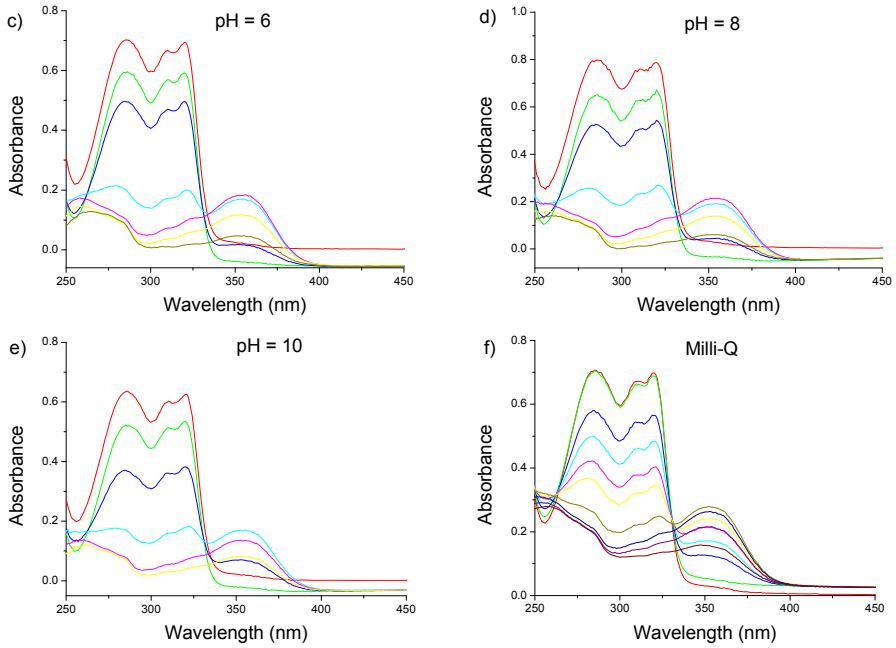

Figure 4.10 (continued): Motor **4.2** (a-e) at varying pH or in unbuffered Milli-Q (f). Stable *trans*-**4.2** (red lines), stable *trans*-**4.2** after 1 week (green lines) and subsequent irradiation (other lines). Despite careful control of analysis conditions, some baseline shifting is observed in several samples.

4.2.4.8 Identification of potential degradation products

To complete the identification of the degradation product of motor **4.2**, a sample of *trans*-**4.2** was dissolved in D_2O and irradiated for 30 min with 312 nm light. The sample was subsequently freeze-dried, redissolved in methanol and submitted for HRMS analysis. A mass of M+19 was measured, which is consistent with the addition of D_2O, followed by exchange of the alcoholic deuterium atom by a hydrogen atom in methanol.

To summarize, the motor **4.2** is stable in water, but upon irradiation it isomerizes and subsequently degrades. However, if the irradiation is halted, the unstable *cis* isomer thermally isomerizes to the stable *cis* isomer in a clean process. The degradation is independent of pH and only occurs in water. The presence of oxygen does not influence the behaviour. A model compound bearing the solubilizing side chain is stable upon irradiation in water. Mass analysis shows that the main degradation product has a mass of M+18. Finally, the degradation product is characterized by a disappearance of UV absorption above 300 nm. These results are consistent with water addition to the double bond, which most likely occurs in a photogenerated intermediate. Such a photoinduced water addition has previously been observed for dihydroquinolines.[24] The double bond in rotary molecular motors is significantly twisted and may also be polarized, rendering it vulnerable to addition reactions. Since this double bond is of key importance to the

design of light-driven rotary molecular motors, we see no immediate solution to this problem. However, by careful choice of reaction conditions, the degradation can be minimized and the rotary cycle can be performed in aqueous environment. Future research might lead to modifications that will render the core double bond less susceptible to nucleophilic attack.

4.2.5 DNA binding assays

In Chapter 2 of this thesis, extensive efforts towards reversible control over DNA structure and function are described. The synthesis of the DNA-motor hybrid reported therein was the most time-consuming part of the investigation. Additionally, the ten-step synthesis could be a limited factor in the production of larger amounts of DNA-bioconjugate. As discussed in Chapter 1 of this thesis, a supramolecular approach towards photocontrol of poly- and oligonucleotides has also produced encouraging results. Particularly reversible DNA/RNA condensation is currently under extensive investigation. The condensation agents discussed in Chapter 1 all share the same structural motif: quarternary ammonium groups. These substituents both serve to solubilize the photoswitches, and to bind to the negatively charged DNA/RNA backbone. Therefore, motor **4.2** seemed to be an ideal candidate to test for DNA binding ability. Figure 4.11 depicts the results of a fluorescence displacement assay. 4',6-Diamidino-2-phenylindole (DAPI) is a groove-binding dye which strongly fluoresces when bound to DNA.[25] In a competitive binding experiment with another binder, DAPI dissociates from the DNA and becomes less fluorescent. Motor **4.2** (both isomers) was mixed with DAPI (0.5 µM) in the presence of oligonucleotide 5'-GCCATATAGCTCTCGCTATATGG-3' (5 µM). At higher concentrations, both *cis* and *trans* isomers could replace the DAPI, resulting in reduced fluorescence. However, at a certain concentration range (~0.1-0.5 µM), *cis*-**4.2** was found to be more effective at binding DNA than *trans*-**4.2**. This result suggests that binding affinity of **4.2** for DNA may be modulated using irradiation. Further research will demonstrate the applicability of molecular motors for photocontrollable DNA binding.

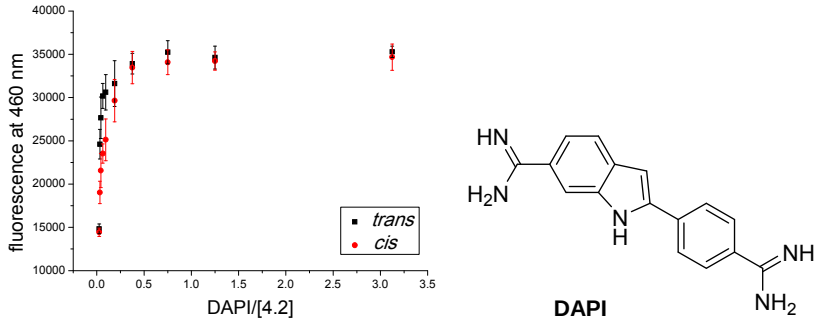

Figure 4.11: Fluorescence displacement assay for motor **4.2** using DAPI stain.

4.3 Motor rotation in micelles

Water soluble motors may find application both inside and outside of the cell. Complimentary to these, applications may be envisioned in which molecular motors need to operate in the biological membrane. All motors reported by our group thus far are only soluble in organic solvents, with the exception of a recent system that was shown to aggregate in water.[9] In theory, many of these may also be operated in a bilayer. To study the operation of molecular motors for use in the cell membrane, a model system was designed. Molecular motor **4.8** (Scheme 4.5) was first reported in 2005.[26] Its photochemical properties are excellent, with high photostationary states and a half-life of 3.17 min. To mimic conditions in a bilayer, motor **4.8** was encapsulated in micelles. Sodium dodecyl sulfate (SDS) was used as the surfactant (CMC = 8.5 mM in water).

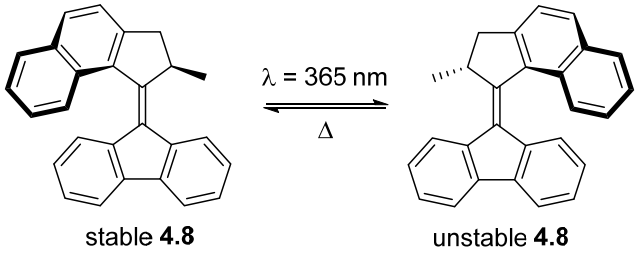

Scheme 4.5: Motor **4.8** and its rotary cycle.

4.3.1 UV-vis spectroscopy

A stock solution of molecular motor **4.8** was film-dried on the inside of a small vial. A 20 mM solution of SDS in aqueous buffer (25 mM Tris, Bis-Tris, MES and sodium acetate, pH= 7.4) was added and the vial was sonicated for 2 min. The final concentration of **4.8** was 20 μM. Initially, the spectrum looked rather poor, with no defined absorptions and absorbance up to 900 nm (Figure 4.12a, black line). However, after several hours at rt, a sharper absorption band could be observed (λ_{max} = 388 nm, Figure 4.12a, red line), which was very similar to the absorbance of **4.8** in hexane (λ_{max} ~ 390 nm). The absorbance at higher wavelengths seen initially may be attributed to scattering effects of larger aggregates of **4.8**. The disappearance of the scattering is indicative of solution of **4.8** in the micelles. The exact same behaviour could be reproduced at various concentrations above the CMC. Irradiation with 365 nm light led to the formation of a new, broader absorption band at a higher wavelength (λ_{max} = 411 nm, Figure 4.12a, blue line), again similar to the absorption corresponding to the unstable isomer in hexane (λ_{max} ~ 420 nm). The clear isosbestic point that can be observed at λ = 406 nm (Figure 4.12b) is indicative of a lack of unwanted side reactions. After leaving the sample at rt for 1 h, the initial spectrum is regenerated (Figure 4.12a, turquoise line), indicating a complete THI to stable **4.8**.

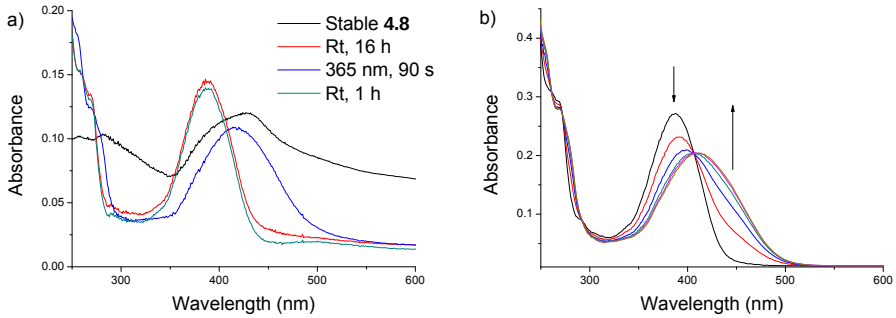

Figure 4.12: UV-vis spectra of motor **4.8** in buffer (25 mM Tris, Bis-Tris, MES and sodium acetate, pH= 7.4) in the presence of SDS. (a) Motor **4.8** (black line), sample after 16 h (red line), PSS (blue line) and after THI (turquoise line). (b) Motor **4.8** upon irradiation with 365 nm light. All spectra recorded at 20 °C under ambient atmosphere.

To confirm that the motor is actually dissolved in micelles, the UV-vis experiment was repeated in PBS buffer (pH = 7.4) only. The UV-vis spectrum initially displayed no defined peaks and absorbance up to 900 nm (Figure 4.13a, black line). Like for the sample containing SDS, the sample was left at rt for 1 day. In the presence of SDS, this leads to a very defined spectrum similar to the UV-vis spectrum of **4.8** in hexane (*vide supra*).[26] Without SDS, the spectrum lowers a little in intensity but retains the same shape (Figure 4.13a, red line). Irradiation with 365 nm light leads to a decrease of the main absorption band and an increase at a higher wavelength. The PSS is reached after 7 min, but a significant absorption at λ_{max} = 406 nm is still present (Figure 4.13b, red line). After leaving the sample at rt for 30 min, minor indication of THI is observed (Figure 4.13b, blue line). After one day at rt, the absorption band at λ_{max} = 406 has somewhat increased in intensity (Figure 4.13b, turquoise line). However, the new absorbance band has not decreased yet. The THI, if occurring at all, seems to be much slower under these conditions. Because the λ_{max} in this spectrum has shifted to a higher wavelength compared the sample containing SDS, the experiment was repeated with a 420 nm LED, but the results were not improved.

Based on the UV-vis experiments, it can be concluded that motor **4.8** both dissolves well and functions properly in SDS micelles. Although some switching behaviour could be observed in aqueous buffer without SDS, the motor is likely not solubilized, which impedes its function.

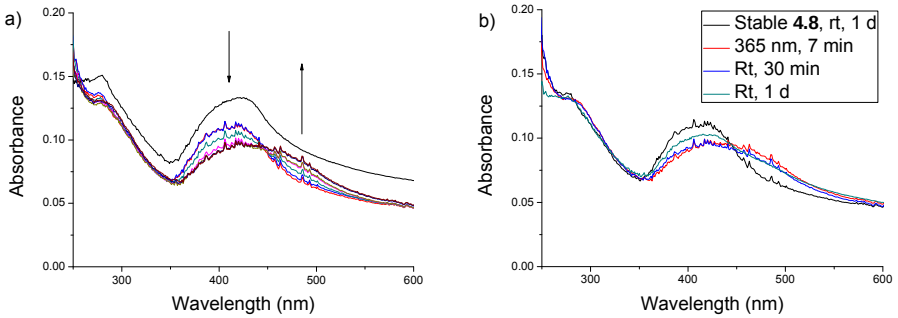

Figure 4.13: UV-vis spectra of motor **4.8** in aqueous buffer (25 mM Tris, Bis-Tris, MES and sodium acetate, pH= 7.4). (a) Motor **4.8** (black line), sample left at rt for 1 day (red line) and upon irradiation with 365 nm light. (b) Motor **4.8** after 24 h (black line), PSS (red line), after 30 min at rt (blue line) and after 1 day at rt (turquoise line). All spectra recorded at 20 °C under ambient atmosphere.

4.3.2 Kinetic analysis

The activation parameters of the THI from unstable **4.8** to stable **4.8** were investigated using Eyring analysis. Samples of motor **4.8** in SDS micelles, in aqueous PBS buffer (pH = 7.4) were irradiated with 365 nm light at several temperatures, until the PSS was reached (1 min). The absorption at 450 nm was then measured over time until the thermal process was complete. All exponential decay lines were fitted using least squares approach. The results were processed using a direct Eyring analysis with errors obtained by a Monte Carlo experiment. The Eyring plot is depicted in Figure 4.14, while calculated activation parameters are listed in the insert. The half-life of **4.8** in micelles at rt was calculated to be 4.93 min, somewhat slower than in hexane (3.17 min).

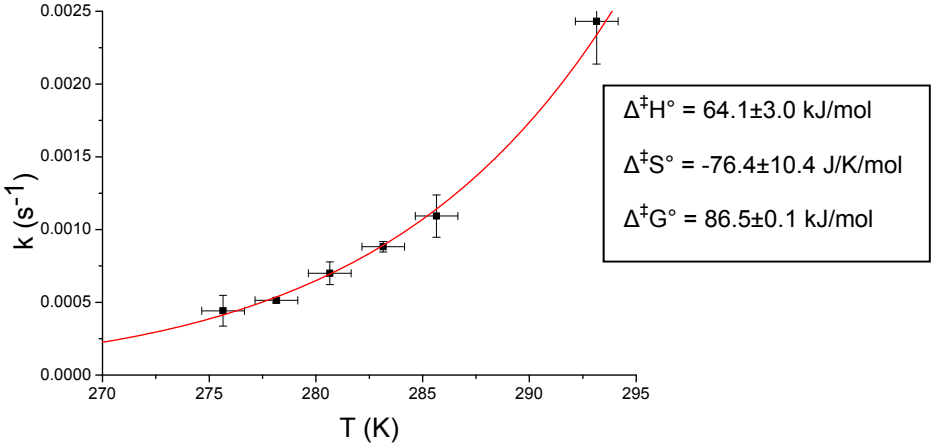

Figure 4.14: Eyring plot of the thermal helix inversion from unstable **4.8** to stable **4.8**, in SDS micelles (20 mM) in aqueous PBS buffer (pH = 7.4), and activation parameters (right).

4.3.3 Viscosity measurements

Motor **4.8** operates somewhat slower in the micelle (4.93 min) than it does in hexane (3.17 min). This is a rather interesting observation, since the inside of a micelle consists of linear aliphatic chains, similar to hexane. Because the natural logarithm of the viscosity is linearly related to the natural logarithm of the THI rate,[27] a longer half-life in the micelle indicates that the internal viscosity is higher than the viscosity of hexane (Chapter 6). It was envisioned that the motor might be used as a probe to monitor the viscosity inside the micelle. A calibration curve was established by measuring the rate of rotation of **4.8** in a range of linear alkanes with increasing viscosity, starting with pentane and ending with dodecane (Figure 4.15, black dots). Notably, the results obtained for **4.8** are different than those reported previously in literature (Figure 4.15, red dot).[26] This difference may arise from the fact that half-lives at rt were recorded in this experiment, while in the previous investigation the activation parameters were obtained by Eyring analysis, from which the half-life at rt was calculated.

Interestingly, increasing viscosity does not seem to affect the rate of rotation of **4.8**, while typically an increasing viscosity will impede the rotation speed. Motor **6.1** (Chapter 6), which was specifically designed to investigate solvent effects on rotation rate, has four butyl side chains, which may significantly increase solvent-solute interactions especially in aliphatic solvents. The lack of these side chains in motor **4.8** may provide a explanation for the absence of a negative correlation between viscosity and rate. The rate of rotation in the micelle is lower than in the aliphatic solvents (Figure 4.15, blue line). Potentially, the density of the aliphatic tails in the micelles is relatively high,[28] which could impede the rotational speed.

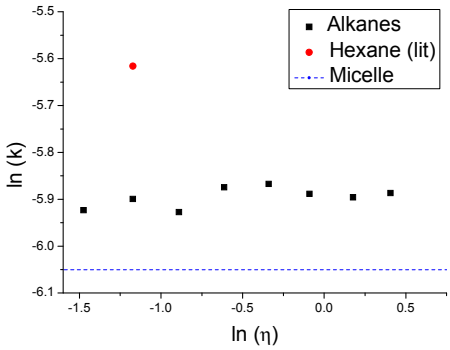

Figure 4.15: Natural logarithm of rate of the THI of **4.8** plotted against natural logarithm of viscosity of the solvent. Because the viscosity inside the micelle is unknown, the measured rate is plotted over the entire axis.

4.3.4 Fatigue resistance

Upon irradiation and subsequent THI of motor **4.8** in 20 mM SDS in buffer (25 mM Tris, Bis-Tris, MES and sodium acetate, pH= 7.4), no degradation of the motor was observed (Figure 4.12b). As discussed earlier in this chapter, the central double bond of a molecular motor is vulnerable to water addition in aqueous environments. Incorporation of the motor in micelles appears to solve this issue. Irradiation with 365 nm light and subsequent THI were repeated for 13 cycles to investigate fatigue resistance of **4.8** in micelles (Figure 4.16). The system was shown to be highly fatigue resistant.

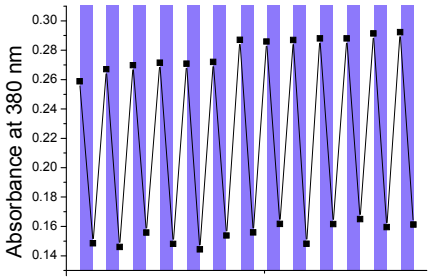

Figure 4.16: Fatigue resistance experiment of motor **4.8** in buffer (pH = 7.4) and 20 mM SDS. Absorbance at 380 nm was monitored after each irradiation with 365 nm light (1 min, purple bands) or THI (rt, 1 h, white bands).Due to duration of experiment, the sample was left at rt overnight, which accounts for the small baseline shift observed between cycles 6 and 7.

4.3.5 UV-vis spectroscopy over a pH range

The stability of motor **4.8** in micelles in aqueous buffer solution was further investigated by operating the motor over a pH range. Figure 4.17 depicts the photochemical behaviour of motor **4.8** in a 20 mM aqueous solution of SDS in buffer (25 mM Tris, Bis-Tris, MES and sodium acetate) at pH = 2, 4, 6, 8 and 10. A UV-vis spectrum was recorded of each sample (black lines) and the samples were irradiated for 1 min with 365 nm light (red lines). Subsequently, all samples were left to undergo THI at rt (blue lines). Spectra of the same samples were recorded after 1 week (turquoise lines) and the experiment was repeated (pink and green lines). Some small baseline shifting was inevitable due to the week long incubation time between the experiments. However, switching function appears to be retained over the entire pH range, and after one week.

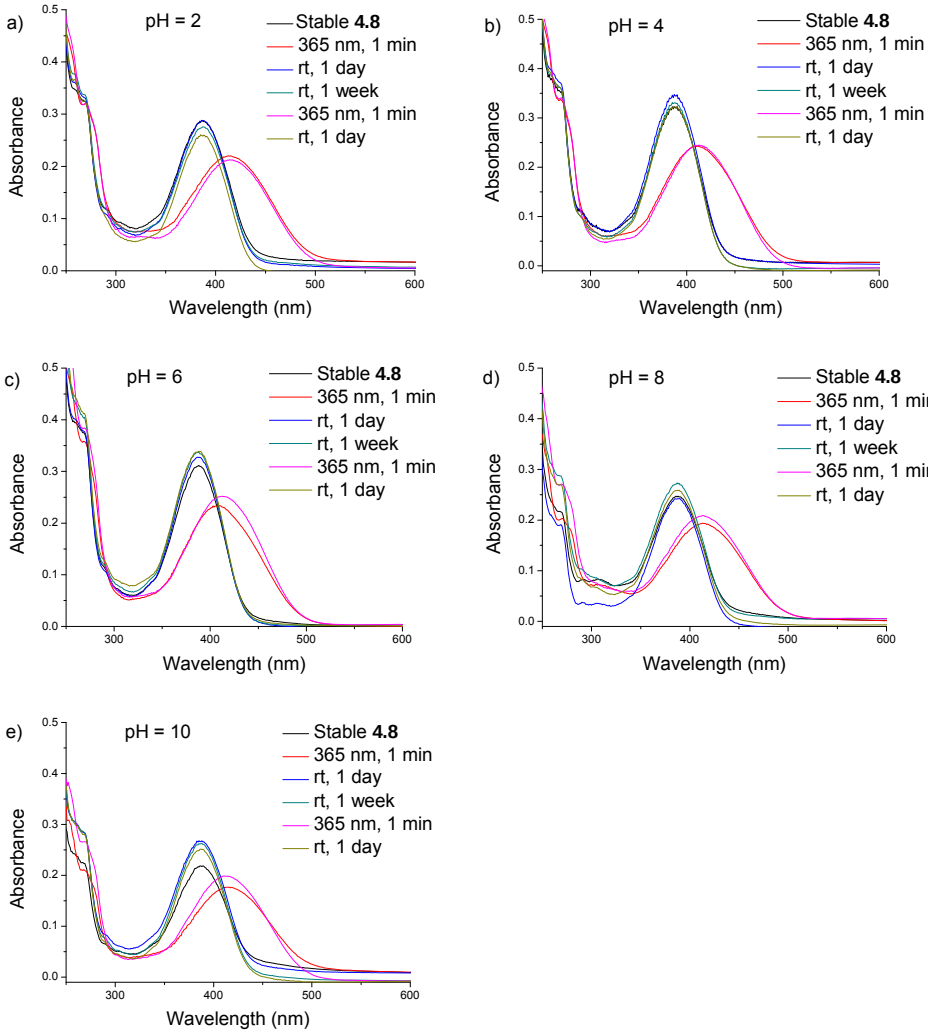

Figure 4.17: Motor stable **4.8** in buffer at varying pH, containing 20 mM SDS. All samples irradiated with 365 nm light for 1 min, followed by THI at rt. All samples subsequently incubated at rt for 1 week, after which the irradiation experiment was repeated.

4.4 Conclusions

In this chapter, two complimentary methods to operate molecular motors under physiological conditions were investigated.

A first-generation motor was functionalized with water solubilizing chains. Although aggregation at higher concentrations can occur, the motor is fully soluble at submillimolar concentrations. The motor displays typical behaviour for first-generation motors and is stable over an extensive pH range. Some degradation can be observed during the switching cycle. Using various techniques, this degradation was attributed to water addition to the double bond, most likely occurring in a photoinduced reaction intermediate deriving from the unstable *cis* isomer. Future research will foremost target synthetic modifications that reduce this degradation. Such investigations are challenging, because the core double bond of the motor is of fundamental importance for the unidirectional rotation. Potentially, electron donating substituents could render the double bond less susceptible for nucleophilic attack.

Additionally, a second generation model molecular motor was operated in micelles, as a model for the cell membrane and other bilayers. The motor shows excellent photochemical properties and does not undergo the same degradation process that is observed for the water-soluble motor because the interior of the micelles forms a protective shell around the motor. The motor can be rotated for at least 13 cycles without significant degradation and is not affected by pH changes. Based on these results, it is expected that most of the molecular motors reported by our group may be operated in a micelle or bilayer.

As demonstrated in Chapters 1, 2, and 5 of this thesis, molecular motors are highly suitable candidates for application in responsive biological systems or photoswitchable drugs. The results presented in this chapter, in particular the realization of a water soluble molecular motor, can provide a starting point for such investigations, and demonstrate that molecular motors are up to this challenge.

4.5 Experimental procedures and acknowledgements

For General Remarks, see Chapter 2. Synthesis of second generation motor **4.8** was performed by Christian Böhmer, under the supervision of Peter Stacko and Filippo Tosi.

2,2',4,4',7,7'-hexamethyl-2,2',3,3'-tetrahydro-[1,1'-biindenylidene]-5,5'-dicarbaldehyde (4.3)

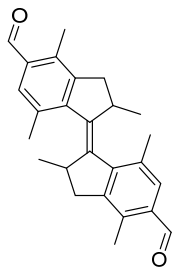

Dibromo-functionalized motor **2.7**[29] (309 mg, 0.652 mmol) was dissolved in dry THF (20 mL) under a nitrogen atmosphere. The solution was cooled to -60 °C and *n*-butyllithium (1.42 mL, 1.6 M solution in hexane, 2.28 mmol) was added dropwise. The mixture was stirred for 1 h at -60 °C. Subsequently, DMF (5.02 mL, 65.2 mmol) was added and the reaction mixture was gradually warmed up to room temperature. The reaction was quenched with a saturated aqueous NH_4Cl solution (20mL). The mixture was extracted with ethyl acetate (3 x 20 mL). The combined organic layers were washed with brine, dried over $MgSO_4$ and concentrated *in vacuo*. The reaction mixture was purified using flash column chromatography (SiO_2, pentane: EtOAc 95:5). *Cis* and *trans* isomers were obtained from the column separately, as a yellow solid and a yellow oil, respectively. The combined product was obtained in 67% yield (140 mg, 0.376 mmol). *Cis:* ^{1}H NMR (400 MHz, $CDCl_3$) δ 10.22 (s, 2H), 7.43 (s, 2H), 3.44 (p, J = 6.8 Hz, 2H), 3.16 (dd, J = 15.1 Hz, 6.3, 2H), 2.60 (m, 8H), 1.53 (s, 6H), 1.10 (d, J = 6.8 Hz, 6H); ^{13}C NMR (101 MHz, $CDCl_3$) δ 192.8, 146.4, 146.1, 143.1, 133.5, 133.5, 133.3, 133.1, 41.7, 38.6, 20.4, 20.3, 14.8; mp: >240 °C (dec.). *Trans:* ^{1}H NMR (400 MHz, $CDCl_3$) δ 10.23 (s, 2H), 7.58 (s, 2H), 2.91 (app. p, 2H), 2.70 (dd, J = 14.8, 5.7 Hz, 2H), 2.51 (s, 6H), 2.50 (s, 6H), 2.38 (d, J = 14.7 Hz, 2H), 1.11 (d, J = 6.8 Hz, 6H); ^{13}C NMR (101 MHz, $CDCl_3$) δ 192.7, 146.2, 144.6, 143.1, 133.7, 133.7, 131.5, 41.9, 38.8, 21.5, 19.1, 14.6. HRMS (APCI): *m/z* calcd for $C_{26}H_{29}O_2$: 373.2162, found 373.2156 ($M+H^+$).

1,1'-(2,2',4,4',7,7'-hexamethyl-2,2',3,3'-tetrahydro-[1,1'-biindenylidene]-5,5'-diyl)bis(*N*,*N*-dimethylmethanamine) (4.4)

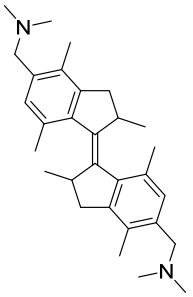

Overcrowded alkene *trans*-**4.3** (76.0 mg, 0.204 mmol) was dissolved in dry DCM (2 mL) under a nitrogen atmosphere. Dimethylamine (408 µL, 2 M in THF, 0.817 mmol) was added and the reaction mixture was stirred at room temperature for 1 h. Subsequently, the reaction mixture was cooled to 0 °C and $NaBH(OAc)_3$ (124 mg, 0.612 mmol) was added. The reaction mixture was warmed up to room temperature and stirred overnight. The reaction was quenched with a saturated aqueous $NaHCO_3$ solution (5 mL) and extracted with ethyl acetate (3 x 5 mL). The combined organic layers were washed with brine, dried over $MgSO_4$ and concentrated *in vacuo*. The product could be purified using flash column chromatography (SiO_2, pentane:EtOAc:NEt_3 95:5:1). Motor *trans*-**4.4** was obtained as a white powder (65 mg, 0.15 mmol, 74%). Motor *cis*-**4.4** could be obtained using the analogous procedure. *Trans:* ^{1}H NMR (400 MHz, $CDCl_3$) δ 6.98 (s, 2H), 3.38 (s, 4H), 2.87 (app. p, 2H), 2.67 (dd, J = 14.5, 5.7 Hz, 2H), 2.42 (s, 6H), 2.29 (s, 12H), 2.24 (d, J = 14.3 Hz, 2H), 2.19 (s, 6H), 1.07 (d, J = 6.4 Hz, 6H); ^{13}C NMR (101 MHz, $CDCl_3$) δ 143.5, 141.3, 140.2, 130.7, 130.6, 130.5, 62.3, 45.9, 42.1, 39.6, 22.1, 19.7, 14.8; mp = 185-188 °C. *Cis:* ^{1}H NMR (400 MHz, $CDCl_3$) δ 6.80 (s, 2H), 3.47 (d, J = 12.5 Hz, 2H), 3.33 (app. p, 2H), 3.25 (d, J = 12.6 Hz, 2H), 3.09 (dd, J = 14.8, 6.3 Hz, 2H), 2.46 (d, J = 14.8 Hz, 2H), 2.27 – 2.23 (m, 18H), 1.47 (s, 6H), 1.06 (d, J = 6.7 Hz, 6H); ^{13}C NMR (101 MHz, $CDCl_3$) δ 144.8, 140.3, 140.0, 135.4, 132.4, 130.1, 129.7, 62.1, 45.5, 41.5, 39.2, 20.5, 20.4, 14.7; mp = 168-169.2 °C. HRMS (AP-CI): *m/z* calcd for $C_{30}H_{43}N_2$: 431.3421, found 431.3414 ($M+H^+$).

1,1'-(2,2',4,4',7,7'-hexamethyl-2,2',3,3'-tetrahydro-[1,1'-biindenylidene]-5,5'-diyl)bis(*N*,*N*,*N*-trimethylmethanaminium) iodide (4.1)

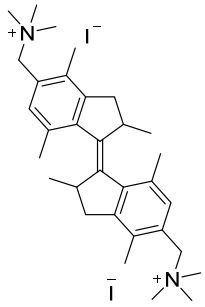

Overcrowded alkene *trans*-**4.4** (20 mg, 0.046 mmol) was dissolved in DCM (2 mL). A large excess of methyl iodide (~100 µL) was added and the mixture was stirred at room temperature. After 30 min, the formed precipitate was filtered off and washed with diethyl ether (5 mL). *Trans*-**4.1** was obtained as a white powder (19 mg, 0.033 mmol, 72%). ^{1}H NMR (400 MHz, DMSO-d6) δ 7.25 (s, 2H), 4.55 (q, J = 13.2 Hz, 4H), 3.06 (s, 18H), 2.84 (t, J = 6.1 Hz, 1H), 2.63 (dd, J = 14.9, 5.7 Hz, 2H), 2.43 (s, 6H), 2.34 (d, J = 14.9 Hz, 2H), 2.26 (s, 6H), 1.05 (d, J = 6.3 Hz, 3H); ^{13}C NMR (101 MHz, DMSO-d6) δ 144.1, 142.0, 141.5, 134.8, 133.23, 130.6, 125.5, 65.0, 51.9, 41.4, 39.2, 21.5, 19.3, 15.6; mp: > 230 °C (decomp). HRMS (ESI): *m/z* calcd for $C_{32}H_{48}N_2$ is 230.19033, found 230.19044 (z=2).

6,6'-bis(2-bromoethoxy)-2,2',4,4',7,7'-hexamethyl-2,2',3,3'-tetrahydro-1,1'-biindenylidene (4.5)

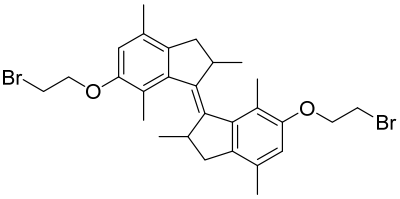

Trans-**4.4** (107 mg, 0.307 mmol) was dissolved in acetonitrile (10 mL). K_2CO_3 (1.06 g, 7.69 mmol) and 1,2-dibromoethane (66.6 µL, 0.769 mmol) were added and the mixture was heated at reflux for 48 h. The reaction mixture was cooled to room temperature and water (20 mL) was added. The mixture was extracted with ethyl acetate (3 x 15 mL) and the combined organic layers were subsequently washed with brine (15 mL), dried over $MgSO_4$ and concentrated *in vacuo*. No further purification was necessary. *Trans* overcrowded alkene **4.5** was obtained as a brown solid (107 mg, 0.226 mmol, 74% yield). *Cis* overcrowded alkene **4.5** could be obtained in analogous manner. *Cis:* ^{1}H NMR (400 MHz, $CDCl_3$) δ 6.53 (s, 2H), 4.25 (app. ddt, 4H), 3.62 (t, J = 6.3 Hz, 4H), 3.34 (app. p, 6H), 3.05 (dd, J = 14.6, 6.3 Hz, 6H), 2.39 (d, J = 14.6 Hz, 6H), 2.25 (s, 6H), 1.41 (s, 6H), 1.07 (d, J = 6.7 Hz, 6H); ^{13}C NMR (101 MHz, $CDCl_3$) δ 155.1, 142.5, 141.2, 137.3, 130.9, 123.1, 112.9, 69.1, 42.0, 38.3, 30.1, 20.6, 19.0, 14.5; mp = 151.8 °C. *Trans:* ^{1}H NMR (400 MHz, $CDCl_3$) δ 6.53 (s, 2H), 4.31 (app. ddt, 4H), 3.71 (t, J = 6.2 Hz, 4H), 2.86 (app. p, 2H), 2.60 (dd, J = 14.2, 5.7 Hz, 2H), 2.33 (s, 6H), 2.18 (app. m, 8H), 1.09 (d, J = 6.4 Hz, 6H); ^{13}C NMR (101 MHz, $CDCl_3$) δ 155.5, 142.8, 141.9, 135.1, 131.6, 121.1, 111.7, 68.7, 42.4, 38.5, 30.1, 19.4, 18.9, 16.4; mp = 151.5 °C. HRMS (ESI): *m/z* calcd for $C_{28}H_{35}Br_2O_2$: 563.0978, found 563.0964 ($M+H^+$).

2,2'-((2,2',4,4',7,7'-hexamethyl-2,2',3,3'-tetrahydro-[1,1'-biindenylidene]-6,6'-diyl)bis(oxy))bis(*N*,*N*,*N*-trimethylethan-1-aminium) (4.2)

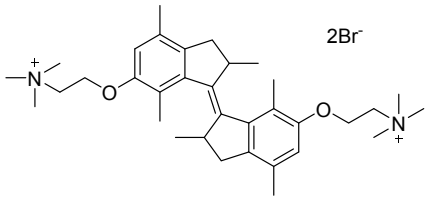

Molecular motor *cis*-**4.5** (49 mg, 0.087 mmol) was mixed with a 4.3 M NMe_3 solution in ethanol (4 mL) in a pressure tube. The tube was closed and the reaction mixture was stirred overnight at 50 °C. After cooling to room temperature, diethyl ether (20 mL) was added to the reaction mixture. The precipitate was filtered off and motor *cis*-**4.2** was obtained as a light brown solid in quantitative yield (59 mg, 0.087 mmol). Motor *trans*-**4.2** could be obtained in an analogous manner. *Cis:* ^{1}H NMR (400 MHz, D_2O) δ 6.64 (s, 2H), 4.30 (app. d, 4H), 3.69 (app. s, 4H), 3.19 (app. d, J = 19.5 Hz, 2H), 3.09 (s, 18H), 2.85 (d, J = 14.3 Hz, 2H), 2.28 (d, J = 15.2 Hz, 2H), 2.10 (s, 6H), 1.19 (s, 6H), 0.85 (d, J = 6.1 Hz, 6H); ^{13}C NMR (101 MHz, D_2O) δ 156.9, 145.2, 144.2, 140.7, 134.7, 124.1, 113.9, 68.1, 65.0, 56.6, 44.4, 40.0, 21.9, 20.2, 16.3; mp: > 310 °C (dec.). *Trans:* ^{1}H NMR (400 MHz, D_2O) δ 6.78 (s, 2H), 4.49 (app. d, 4H), 3.89 (app. s, 4H), 2.77 (app. t, 2H), 2.43 (app. d, 2H), 2.29 (s, 6H), 2.22 (d, J = 14.8 Hz, 2H), 2.16 (s, 6H), 1.03 (d, J = 6.3 Hz, 6H); ^{13}C NMR (101 MHz, D_2O) δ 157.5, 145.0, 144.5, 137.9, 135.1, 122.9,

113.8, 68.1, 65.0, 56.7, 44.4, 39.8, 20.8, 20.0, 18.4; mp: >240 °C (dec.). HRMS (ESI): *m/z* calcd for $C_{34}H_{52}N_2O_2$: 260.2009, found 260.2005 (*z*=2).

N,*N*,*N*-trimethyl-2-(naphthalen-1-yloxy)ethan-1-aminium bromide (4.7)

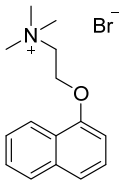

1-(2-bromoethoxy)naphthalene (118 mg, 0.472 mmol) was mixed with a 4.3 M NMe_3 solution in ethanol (5 mL) in a pressure tube. The tube was closed and the reaction mixture was stirred overnight at 50 °C. After cooling down to room temperature, diethyl ether (20 mL) was added to the reaction mixture. The precipitate was filtered off and model compound **4.7** was isolated as a yellow powder (86 mg, 0.28 mmol, 60%). ^{1}H NMR (400 MHz, D_2O) δ 8.18 (d, *J* = 8.0 Hz, 1H), 7.91 (d, *J* = 7.8 Hz, 1H), 7.55 (m, 3H), 7.47 (t, *J* = 8.1 Hz, 1H), 7.00 (br. d, *J* = 5.4 Hz, 1H), 4.67 (br. s, 2H), 3.96 (br. s, 2H), 3.28 (s, 9H); ^{13}C NMR (101 MHz, D_2O) δ 155.4, 136.8, 130.3, 129.6, 128.9, 128.7, 127.2, 123.9, 123.8, 108.0, 67.9 (t), 64.4, 56.5 (t); mp = 198 °C. HRMS (ESI): *m/z* calcd for $C_{15}H_{20}NO$: 230.1539, found 230.1542.

9-(2-methyl-2,3-dihydro-1H-cyclopenta[a]naphthalen-1-ylidene)-9H-fluorene (4.8)

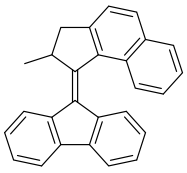

Second generation motor **4.8** was synthesized according to literature procedure in 45% yield (188 mg, 0.556 mmol).[26] ^{1}H NMR (400 MHz, $CDCl_3$) δ 8.10 – 8.04 (m, 1H), 8.00 (d, *J* = 8.2 Hz, 1H), 7.97 (d, *J* = 8.2 Hz, 1H), 7.95 – 7.89 (m, 1H), 7.86 (d, *J* = 8.5 Hz, 1H), 7.83 (d, *J* = 7.5 Hz, 1H), 7.63 (d, *J* = 8.2 Hz, 1H), 7.52 (t, *J* = 7.5 Hz, 1H), 7.49 – 7.43 (m, 2H), 7.38 (dt, *J* = 7.3, 0.9, 0.0 Hz, 1H), 7.28 (td, *J* = 7.5, 1.0 Hz, 1H), 6.89 (t, *J* = 7.5 Hz, 1H), 6.84 (t, *J* = 9.1 Hz, 1H), 4.42 (p, *J* = 6.6 Hz, 1H), 3.63 (dd, *J* = 15.0, 5.6 Hz, 1H), 2.81 (d, *J* = 15.1 Hz, 1H), 1.45 (d, *J* = 6.7 Hz, 3H); ^{13}C NMR (101 MHz, $CDCl_3$) δ 151.1, 147.4, 140.1, 139.8, 139.5, 137.1, 136.3, 132.6, 130.8, 130.4, 129.8, 128.6, 127.5, 126.9, 126.9, 126.9, 126.5, 125.9, 125.8, 125.3, 124.1, 124.0, 119.7, 118.9, 45.5, 41.9, 19.3; mp = 150-152 °C; HRMS (ESI): *m/z* calcd for $C_{27}H_{21}$: 345.1638, found 345.1635 ($M+H^+$).

4.6 References

1 N. Koumura, R. W. Zijlstra, R. A. van Delden, N. Harada, B. L. Feringa, *Nature* **1999**, *401*, 152–155.
2 N. Koumura, E. M. Geertsema, M. B. van Gelder, A. Meetsma, B. L. Feringa, *J. Am. Chem. Soc.* **2002**, *124*, 5037–5051.
3 J. Vicario, M. Walko, A. Meetsma, B. L. Feringa, *J. Am. Chem. Soc.* **2006**, *128*, 5127–5135.
4 M. Klok, M. Walko, E. M. Geertsema, N. Ruangsupapichat, J. C. M. Kistemaker, A. Meetsma, B. L. Feringa, *Chem. Eur. J.* **2008**, *14*, 11183–11193.
5 J. Wang, B. L. Feringa, *Science* **2011**, *331*, 1429-1432.
6 R. Eelkema, M. M. Pollard, J. Vicario, N. Katsonis, B. S. Ramon, C. W. M. Bastiaansen, D. J. Broer, B. L. Feringa, *Nature* **2006**, *440*, 163.
7 M. Vlatkovic, B. L. Feringa, S. J. Wezenberg, *Angew. Chem. Int. Ed.* **2016**, *55*, 1001–1004.
8 S. J. Wezenberg, C. M. Croisetu, M. C. A. Stuart, B. L. Feringa, *Chem. Sci.* **2016**, *7*, 4341–4346.
9 D. J. van Dijken, J. Chen, M. C. A. Stuart, L. Hou, B. L. Feringa, *J. Am. Chem. Soc.* **2016**, *138*, 660–669.
10 C. Poloni, M. C. A. Stuart, P. van der Meulen, W. Szymanski, B. L. Feringa, *Chem. Sci.* **2015**, *6*, 7311–7318.
11 R. A. van Delden, M. K. J. ter Wiel, M. M. Pollard, J. Vicario, N. Koumura, B. L. Feringa, *Nature* **2005**, *437*, 1337–1340.
12 G. London, G. T. Carroll, T. Fernández Landaluce, M. M. Pollard, P. Rudolf, B. L. Feringa, *Chem. Commun.* **2009**, 1712–1714.
13 K.-Y. Chen, S. J. Wezenberg, G. T. Carroll, G. London, J. C. M. Kistemaker, T. C. Pijper, B. L. Feringa, *J. Org. Chem.* **2014**, *50*, 10690–10697.
14 T. Kudernac, N. Ruangsupapichat, M. Parschau, B. Maciá, N. Katsonis, S. R. Harutyunyan, K.-H. Ernst, B. L. Feringa, *Nature* **2011**, *479*, 208–211.
15 W. A. Velema, W. Szymanski, B. L. Feringa, *J. Am. Chem. Soc.* **2014**, *136*, 2178–2191.
16 J. C. M. Kistemaker, P. Štacko, J. Visser, B. L. Feringa, *Nat. Chem.* **2015**, *7*, 890–896.
17 K.-Y. Chen, O. Ivashenko, G. T. Carroll, J. Robertus, J. C. M. Kistemaker, G. London, W. R. Browne, P. Rudolf, B. L. Feringa, *J. Am. Chem. Soc.* **2014**, *136*, 3219–3224.
18 F. Nagatsugi, Y. Takahashi, M. Kobayashi, S. Kuwahara, S. Kusano, T. Chikuni, S. Hagihara, N. Harada, *Mol. Biosyst.* **2013**, *9*, 969–73.
19 S. J. Wezenberg, M. Vlatkovic, J. C. M. Kistemaker, B. L. Feringa, *J. Am. Chem. Soc.* **2014**, *136*, 16784–16787.
20 T. van Leeuwen, J. Gan, J. C. M. Kistemaker, S. F. Pizzolato, M. C. Chang and B. L. Feringa, *Chem. Eur. J.* **2016**, *22*, 7054–7058.
21 P. Greenspan, S. D. Fowler, *J. Lipid Res.* **1985**, *26*, 781–789.
22 X. Guo, X. Ma, Q. Yang, J. Xu, L. Huang, J. Jia, J. Shan, L. Liu, W. Chen, H. Chu, J. Wei, X. Zhang, H. Sun, Y. Tang, Q. You, *Eur. J. Med. Chem.* **2014**, *81*, 89–94.
23 S. O. Sablin, M. J. Krueger, V. L. Yankovskaya, S. E. Tkachenko, A. N. Razdolsky, S. O. Bachurin, R. R. Ramsay, T. P. Singer, *J Biochem. Toxicol.* **1996**, *11*, 33–43.
24 T. D. Nekipelova, V. S. Shishkov, V. A. Kuzmin, *High Energy Chem.* **2002**, *36*, 183–188.
25 J. Kapuscinski, *Biotech. Histochem.* **1995**, *70*, 220–233.
26 J. Vicario, A. Meetsma, B. L. Feringa, *Chem. Commun.* **2005**, 5910–5912.
27 D. Gegiou, K. A. Muszkat, E. Fischer, *J. Am. Chem. Soc.* **1968**, *90*, 12–18.
28 D. Stigter, *J. Colloid Interface Sci.* **1967**, *23*, 379–388.
29 T. M. Neubauer, T. van Leeuwen, D. Zhao, A. S. Lubbe, J. C. M. Kistemaker, B. L. Feringa, *Org. Lett.* **2014**, *16*, 4220–4223.